THE ASTROPHYSICAL JOURNAL, 387:83–94, 1992 March 1

INSTABILITIES IN ASTROPHYSICAL JETS. II. NUMERICAL SIMULATIONS OF SLAB JETS

JUN-HUI ZHAO
National Radio Astronomy Observatory,[1] P.O. Box O, Socorro, NM 87801;[2] and Institute for Astrophysics, University of New Mexico, Albuquerque, NM 87131

JACK O. BURNS
Department of Astronomy, New Mexico State University, Las Cruces, NM 88003

MICHAEL L. NORMAN
National Center for Supercomputing Applications and Department of Astronomy, The Beckman Institute, University of Illinois, Urbana, IL 61801

AND

MARTIN E. SULKANEN
X-Ray Astronomy Branch, Space Science Laboratory, NASA/Marshall Space Flight Center, Huntsville, AL 35812
Received 1990 October 5; accepted 1991 August 30

ABSTRACT

In this paper, we describe numerical simulations of an unstable supersonic slab-symmetric jet. The instabilities within the jet are characterized by growing internal body waves and their coupled surface waves that are also predicted in linear perturbation theory. The characteristic theory of fluid dynamics is used to help interpret the wave morphologies. We demonstrate that these waves can be excited by imposing an arbitrary disturbance. From our numerical simulations, we find that the sound waves propagating against the flow slow down as they propagate outward, and they grow in amplitude. These waves eventually disrupt the jet at a certain length. This disruption length is related to the jet Mach number and the perturbation intensity. Thus, the Mach number of a jet observed with a radio telescope can be estimated by measuring the disruption length and estimating the perturbation intensity. The jet Mach numbers in radio tailed sources determined in this way agree quite well with estimates from ram pressure bending arguments. The wiggles and flares observed in many extragalactic jets, especially in tailed radio sources, appear to be intimately related to instabilities and the jet disruption process.

Subject headings: galaxies: jets — hydrodynamics — instabilities — methods: numerical — shock waves

1. INTRODUCTION

Over the past two decades, astrophysical jets have been extensively studied in the context of fluid dynamics (e.g., Begelman, Blandford, & Rees 1984, hereafter BBR). Instabilities in astrophysical jets were viewed as being important (Scheuer 1974; Blandford & Rees 1974) in early jet models. The effects of Kelvin-Helmholtz (K-H) instabilities on the propagation of a jet have been emphasized by BBR. In particular, they noticed that the weak, edge-darkened sources (or tailed sources) found commonly in galaxy clusters may be fueled by beams that have been decelerated by surface instabilities, and the disruption or decollimation of their jets may be caused by nonlinear development of Kelvin-Helmholtz instabilities.

A typical example of a narrow-angle tailed (NAT) radio source is NGC 1265 (Miley et al. 1972; O'Dea & Owen 1986). Recent high-resolution radio observations show that well-collimated jets, emanating from the nucleus of a NAT radio galaxy, are strongly bent before they suddenly disruption or transform into plumelike tails. Begelman, Rees, & Blandford (1979) and Jones & Owen (1979) proposed twin-jet models to explain this morphology. In these models, the jets are bent by ram pressure arising from transonic motion through the intergalactic medium. These bending models explain the curved jets but the decollimation problem remains unsolved. Can this jet/tail transition be explained by the onset of K-H instabilities? Another class of cluster radio galaxies, wide-angle tailed (WAT) sources (O'Donoghue, Owen, & Eilek 1990, hereafter OOE), also show the abrupt transition from well-collimated jets into diffuse tails. Some of the jets appear to wiggle with large amplitude prior to the disruption (e.g., 0110+152, OOE; 3C449; Perley, Wills, & Scott 1979). Figure 1 presents a high-resolution VLA image of a prototype of WAT. In contrast to classical doubles (e.g., Cygnus A; Perley, Bridle, & Willis 1984), tailed radio sources appear more complex, are edge-darkened, and lack hot spots at the outer extremities of the two extended lobes. The abrupt disruptions of WAT jets can not be simply understood by a conventional "working surface" model which is, in fact, successful in explaining of the formation of hot spots in classical doubles (e.g., Smith et al. 1985). The jet wiggles and the sudden jet disruptions in tailed radio sources may be visible symbols of growing waves due to K-H instabilities developed in the jets.

Recently, efforts have been made by a number of authors to understand the K-H instability and the instability mode structures in a jet. Previous linear analysis predicted that a thermally confined jet is unstable to a variety of growing modes (Ferrari, Trussoni, & Zaninetti 1981; Payne & Cohn 1985; Hardee & Norman 1988). However, there are some difficulties comparing the individual modes given by previous linear results with either numerical simulations or observed astrophysical jets.

In a companion paper (Zhao et al. 1991 hereafter Paper I), we have developed a technique to examine the individual

[1] The National Radio Astronomy Observatory is operated by Associated Universities, Inc., by cooperative agreement with the National Science Foundation.
[2] Postal address.

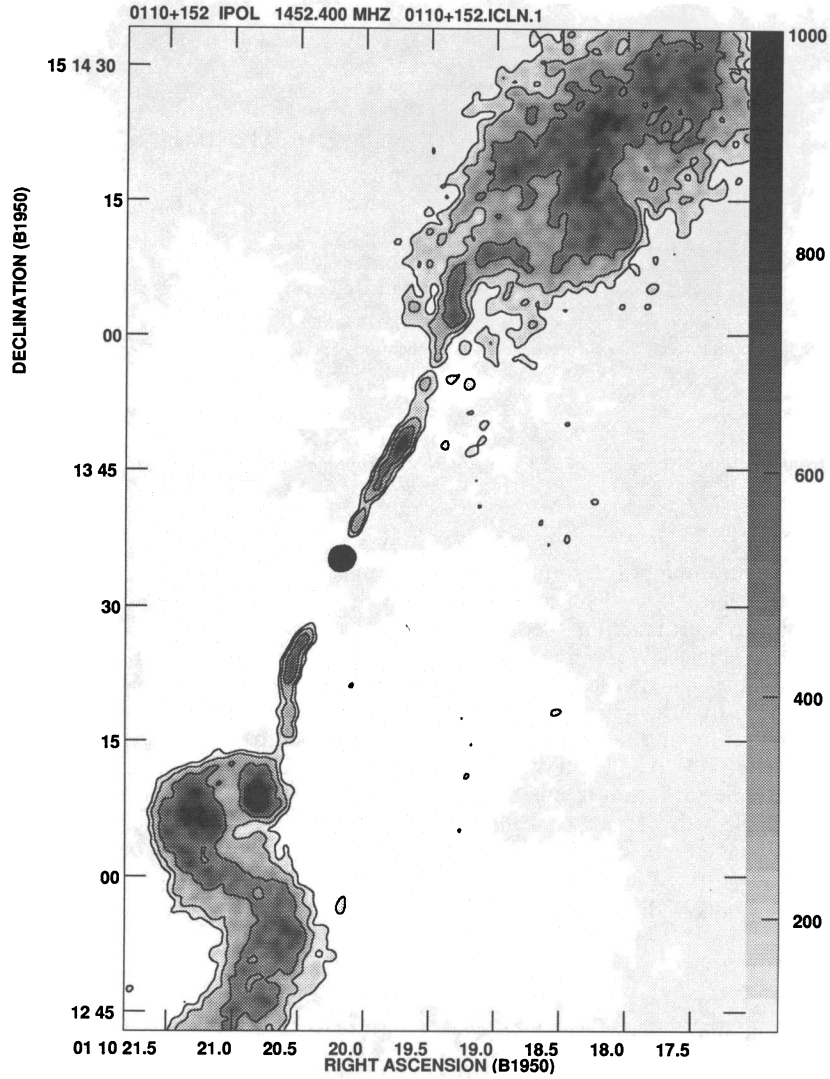

FIG. 1.—High-resolution (1″) image of jets and inner tails of 0110+152. It shows the collimated jets, wiggles, and abrupt jet/tail transitions in a WAT. Gray-scale flux density range is 100–1000 μJy beam^{-1}. Peak flux density is 4.73×10^{-3} Jy beam^{-1}. Contour levels are 4, 8, 16, 32, 64, 128, and 256 $\times$ 30 μJy beam^{-1}. We acknowledge Aileen O'Donoghue for providing us with this figure, and interested readers should see the paper written by O'Donoghue, Owen, & Eilek (1990) for more details.

modes of different kinds of wave packets. We formulated a scheme for tracing the nonlinear development of these waves to explore the effects of K-H interface instabilities on jet propagation and decollimation. An understanding of the wave characteristics is crucial for comparing the results from linear theory with numerical simulations and astrophysical observations. In this paper, we show that perturbation waves can grow in a thermally confined jet, and the waves essentially disrupt the jet.

The remainder of this paper is organized as follows. In § 2, we review previous numerical simulations of astrophysical jets. In § 3, we describe the numerical method and initial setup for the simulations discussed in this paper. In § 4, we analyze and discuss the results from our numerical simulations. In § 5, we describe the astrophysical implications of our numerical simulations. Section 6 presents a summary and conclusions.

2. RESULTS OF PREVIOUS NUMERICAL SIMULATIONS

Recent high-resolution interferometer observations (e.g., VLA, WSRT, MERLIN, and VLBI network) of extragalactic radio sources reveal jetlike structure. Various attempts have been made to explore the nature of these radio sources. Most of the basic features can be modeled by hydrodynamic and/or MHD simulations (e.g., Norman et al. 1982; Norman, Winkler & Smarr 1984; Williams & Gull 1984, 1985; Wilson & Falle 1983; Norman & Winkler 1986; Arnold & Arnett 1986; Clarke, Norman, & Burns 1986, 1989; Norman & Hardee 1988; Lind et al. 1989; Mathews & Scheuer 1990a, b; Hardee & Norman 1990; Cox, Gull, & Scheuer 1991; Hardee et al. 1992).

Instabilities and disruptions of jets have now been seen in a variety of numerical simulations. In fact, the body and the relevant surface waves propagating against the flow have been observed as a fast-growing wave pattern in jet simulations (Norman et al. 1984). The speed given by Norman et al. is systematically smaller than $u_0 - a_{\rm in}$ (suggested by linear theory; see Paper I) because their measurements were made in a partially nonlinear stage. The waves in that stage become nonlinear and the jet starts to disrupt. The propagation of the body waves substantially slow down because of nonlinear

developments of instabilities. The body and the relevant surface waves propagating along the flow can been ignored because they are rarefied in density and are dispersive. In other words, the body waves propagating along the jet are relatively unimportant in jet disruptions.

Recently, Norman & Hardee (1988, hereafter NH) performed extensive numerical simulations to search for the particular growing modes predicted in the linear theory. In general, their comparison between the simulations and linear theory is not exact since their numerical simulations are well developed nonlinear flows. However, they found very interesting phenomena associated with jet disruption. One remarkable result is that jets with an imposed sinusoidal oscillation perturbation are disrupted at or near the resonant wavelength (which is defined by Hardee & Norman 1988) as the wavelength corresponding to the maximum growth rate in those fixed real frequency modes) of the fundamental sinusoidal mode, independent of the driving frequency. Their results imply that any kind of perturbation imposed within a jet may grow and lead to the disruption of collimation. According to the linear analysis in Paper I, two types of waves, body and surface waves, exist in a fluid system with an interface between two different kinds of fluid defined by density, velocity, etc. It is useful to classify jet instabilities in terms of body and surface waves because a perturbed jet, in general, is characterized by these waves. The relationship between these waves and growing modes found in previous studies was not clear. However, it motivated us to carry out a generalized linear study of the instabilities in astrophysical jets and directly compare the results from the linear analysis with numerical simulations. In contrast to NH's simulations, we investigated the excitations and linear developments of the waves with different kinds of perturbation. We are most concerned with the dynamical evolution of the waves at linear and early nonlinear stages in the simulations.

3. THE NUMERICAL METHOD

ZEUS is a two-dimensional, second-order accurate astrophysical fluid dynamics code (Norman & Winkler 1986), under development at the National Center for Supercomputing Applications. The code is explicit in time, solving the hydrodynamic equations on an Eulerian grid in either Cartesian, cylindrical, or spherical polar coordinates. The slab-geometry jet simulations were computed on a 400 × 400 grid zone mesh in Cartesian coordinates. There were 20 uniform grid zones across the jet in r-direction, which sufficiently resolves the inner structure of the jet. The inner 200 radial zones were uniform. The outer 100 radial zones on either side of the jet increased in size geometrically, so that the entire grid was also 80 jet radii wide. The grid was 80 jet radii long in the z-direction.

We set up an initially steady jet flowing through a jet channel, pressure-balanced with the ambient gas. The initial velocity, density, and pressure of the jet are specified by u_0, ρ_{in}, and p_{in}, respectively. The ambient gas is static with density (ρ_{ex}) and pressure (p_{ex}). We designed two different velocity perturbations (A and B) that we imposed on the jets. In case A, which is similar to NH's simulations, the slab jet was driven by a periodic sinusoidal oscillation of the r-component of the jet's velocity. The maximum amplitude of the transverse velocity was $u_r/u_0 = 0.01$, where u_0 is the velocity of the steady flow in the z-direction. In case B, instead of the periodic sinusoidal oscillation, we imposed an r-direction perturbation of the jet velocity with $u_r/u_0 = 0.01$ at the inlet on the left edge of the grid. Case B was fully independent of any driving frequency. Illustrations of these perturbations are shown in Figure 2. Thus, we were able to directly compare the two cases to show that the disruption of the jet is caused by the self-excited modes rather than a driven mode.

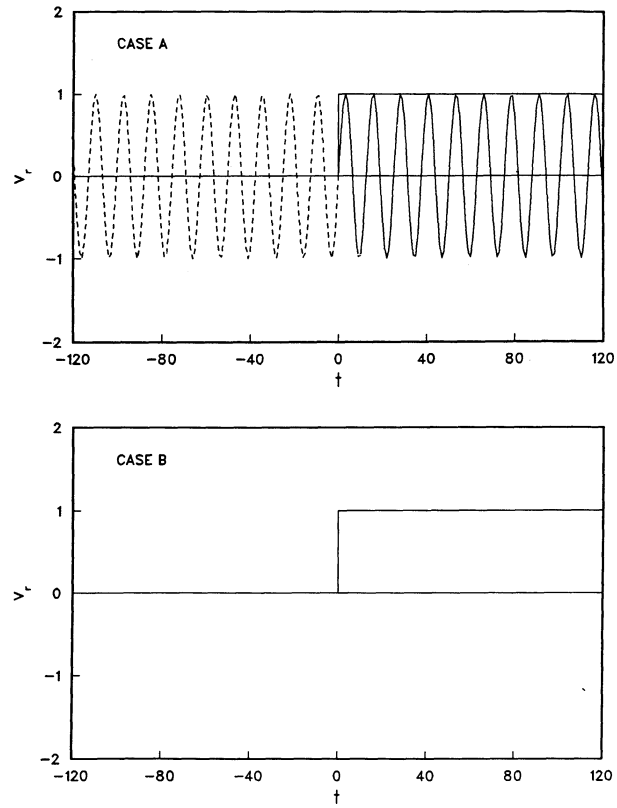

FIG. 2.—Temporal behavior of imposed perturbations on jet inlet in the simulations. Case A: sinusoidal function modulated by a step function. Case B: step function only.

In order to compare the differences caused by different perturbations, we designed two simulations with the same physical parameters for the jet and ambient gas but with different perturbations as mentioned above. The ratio of the jet density to ambient density ($\eta = \rho_{in}/\rho_{ex}$) was 0.1. The internal Mach number (M_{in}) was 3 and the external Mach number (M_{ex}) was 9.5. The jet material flows into the jet channel which is in pressure balance with the ambient. The physical parameters η, M_{in}, and M_{ex} in the following simulations are the same as in NH's simulations A, B, and C except we used astrophysical units in the calculation instead of the grid units used in NH's simulations. In Table 1, we list the parameters used in the simulations.

TABLE 1

THE PHYSICAL PARAMETERS IN SIMULATIONS OF A SLAB JET (CASES A AND B)

Parameter	ρ^a (cm^{-3})	M_{in}	$u_0{}^b$ (km s^{-1})	R (kpc)	a (km s^{-1})
Jet	10^{-4}	3	10^4	2	3333
Ambient	10^{-3}	...	0	...	1054

[a] ρ is gas density; M_{in} is jet internal Mach number.
[b] u_0 is jet velocity; R is jet radius; a is sound speed.

4. NUMERICAL SIMULATIONS AND DISCUSSIONS

In Paper I, we found a number of waves associated with growing modes existing in a thermally confined slab jet. Our linear analysis indicates that the growing modes are intrinsic to the system and can be excited by an arbitrary disturbance imposed on the jet. These waves are expected to propagate along the jet and grow in amplitude. In what follows, we will examine the predictions made by linear theory with our nonlinear simulations.

4.1. *"Switching-on" Effect of Imposing Perturbation*

Investigation of different perturbations in numerical simulations is helpful in understanding the disruption process in astrophysical jets. In NH's simulations, the authors studied the effect of different oscillation frequencies on the stability of a slab jet. They mainly concentrated on a comparison of the nonlinear behavior and the morphology. In those simulations performed by NH, the jets with different driving frequencies show very similar morphology and disruption behavior at the early simulation times. This indicates that there are common characteristics of these imposed disturbances.

From Fourier theory, we know that the nature of a perturbation is important in determining what kind of modes will be initially excited. Spatially, a perturbation imposed at the jet inlet is just like a δ-function in the z-axis, $\delta(z)$, which is composed of many, equally weighted spatial modes. Temporally, the perturbation used in NH's simulation is not a perfect sinusoidal oscillation. What they used is a sinusoidal oscillation modulated by a step function which switches on a perturbation (see Fig. 2*a*). However, the perturbation is no longer a monofrequency oscillation since the modulated step function contains all possible frequency modes with a certain weighting function. We suggest that the simulations (A, B, C) in NH are similar at the beginning (or linear stage) because the step function may excite all the intrinsic modes which form the waves in the system. The system responding to the sinusoidal oscillation is expected to be seen only at a long time after initially transient modes propagate away (Gaster 1965), which actually has been observed by NH. To further verify these ideas, we designed a simulation with a simple step function (see Fig. 2*b*) perturbation to compare with the sinusoidal oscillation.

In Figure 3 (Plate 1), we present a number of density images of a slab jet at different times in the evolution. Note that these images are from the early simulation times. Figure 3 contains two simulations of the same jet with different perturbations (cases A and B). Figure 3*a* corresponds to case A with a sinusoidal oscillation modified by a step function. Figure 3*b* corresponds to case B with a step function only (see Fig. 2). Thus, we are able to directly compare the excitation process and the internal structures in the two runs. In the two cases, the jet is in general characterized by the same growing wave patterns corresponding to sound waves propagating with and against the flow which we have discussed in Paper I. The leading fronts of the waves in both cases A and B are identical. Thus, an important conclusion drawn from Figure 3 is that the step function plays the dominant role in exciting the initial wave modes.

4.2. *Growing Waves and Jet Disruption*

NH's study concentrated on the effects of different oscillation frequencies on the stability of a slab jet. Here, we mainly examine the linear growth behavior of the resonant waves in a slab jet. We trace the evolution of the jet at a very small time period from $t = 5$ (in time units of $\Delta t = 4 \times 10^{12}$ s $\approx 1.27 \times 10^5$ yr that correspond to the time separation between two successive images; hereafter we use Δt as the unit of time) to $t = 95$. In Figure 3, we present density images of a slab jet at different stages of evolution. Figure 4 contains the relevant one-dimensional density profiles along the internal central axis of the jet.

The jet is characterized by two distinguishable wave patterns propagating along two characteristic lines in the space and time (z, t)-plane. First, the faster propagating wave pattern is a rarefied wave (see Fig. 4) and its amplitude in density is less than the steady background flow. Comparing the minimum density of the wave between two successive epochs, we find that the wave grows in amplitude. The wave also spreads over a wider range in the jet as time increases, which indicates that the wave is dispersed. In Table 2, our measurements for the central velocities as well as the velocity dispersion for the fast moving pattern are listed. The average central velocity of the pattern is $1.33 \pm 0.04\ u_0$, which agrees very well with the predicted theoretical velocity ($u_0 + a = 4/3\ u_0$) for an internal sound wave propagating with the flow in a $M_{\rm in} = 3$ jet from Paper I. The wave has an average velocity dispersion of $0.25 \pm 0.03\ u_0$ which also has been suggested in linear theory (see Fig. 11 in Paper I), but the range of the dispersed velocities is smaller than that expected by our linear analysis. Also, the growth of the wave is much slower than expected by linear perturbation theory. The difference between linear theory and numerical calculation is caused by the finite grid in the numerical calculations. Thus, the fast and/or the high-frequency modes (or wave components) are truncated in the numerical simulations.

Second, the most important feature in the jet with regard to disruption is the slow propagating pattern. This wave pattern is dominated by components which are compressed (or condensed) in density relative to the undisturbed steady flow. Our measurements of the speed for the slow-moving pattern are listed in Table 2. The average propagating velocity of the wave is about ($0.67 \pm 0.04\ u_0$) at a linear phase ($t \leq 55$ approximately), which again is consistent with the predictions made by linear theory (in Paper I). The velocity dispersion of the wave is $\sim 1.1\ u_0$ which agrees with the linear prediction (see Fig. 11 in Paper I). The crucial characteristic of this wave pattern is much faster growth than the fast-moving pattern. After $t = 55$, the wave grows significantly and the propagation slows. The increased amplitude of the relevant surface waves

TABLE 2

PROPAGATION VELOCITY AND VELOCITY DISPERSION OF WAVE PATTERNS

	Fast Pattern		Slow Pattern	
t (unit[a])	u_p/u_0	$\Delta u_p/u_0$	u_p/u_0	$\Delta u_p/u_0$
5.....	1.30	...	...	...
15.....	1.27	0.20	0.63	<1.03
25.....	1.30	0.30	0.64	<1.13
35.....	1.31	0.29	0.71	<1.10
45.....	1.37	0.25	0.71	<1.03
55.....	1.31	0.24	0.66	<1.03
65.....	1.36	0.23	0.60	<1.07
75.....	1.36	0.24	0.55	<1.06
85.....	1.38	0.27	0.51	<1.15
95.....	...	...	0.48	<1.19

[a] Unit = 4×10^{12} s $\approx 1.27 \times 10^5$ yr.

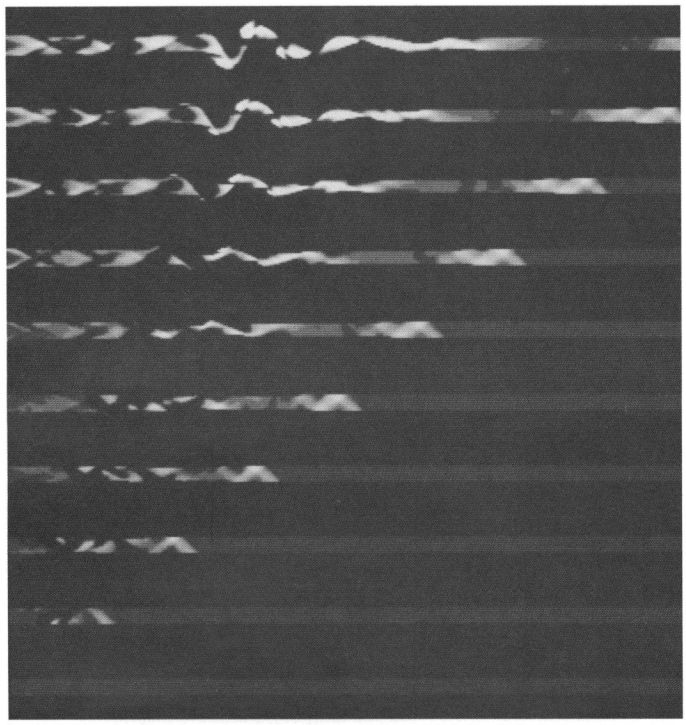

FIG. 3*a*

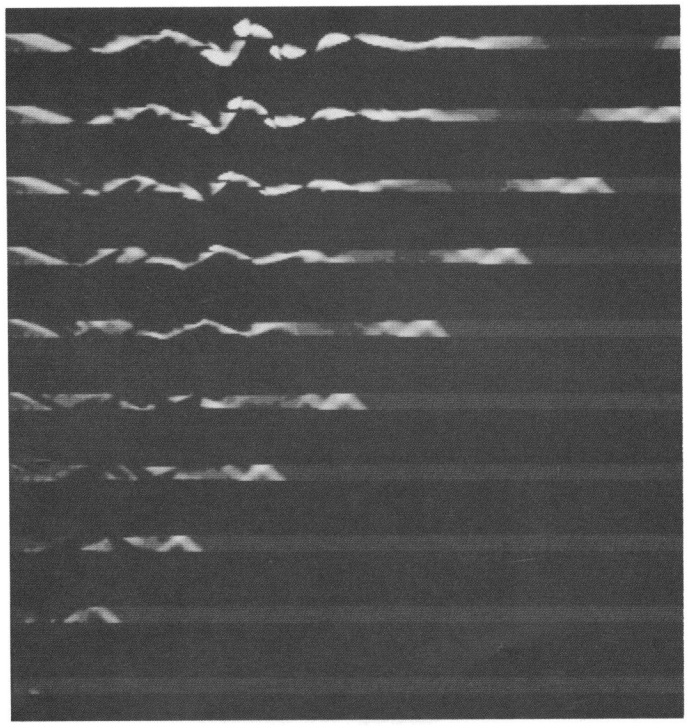

FIG. 3*b*

FIG. 3.—(*a–b*) The internal body waves and surface waves excited by different perturbations (cases A and B) described in Fig. 2. The jet slots are produced at simulation times 5, 15, 25, 35, 45, 55, 65, 75, 85, 95 (in units of 4×10^{12} s = 1.27×10^5 yr from bottom to top).

ZHAO et al. (see 387, 86)

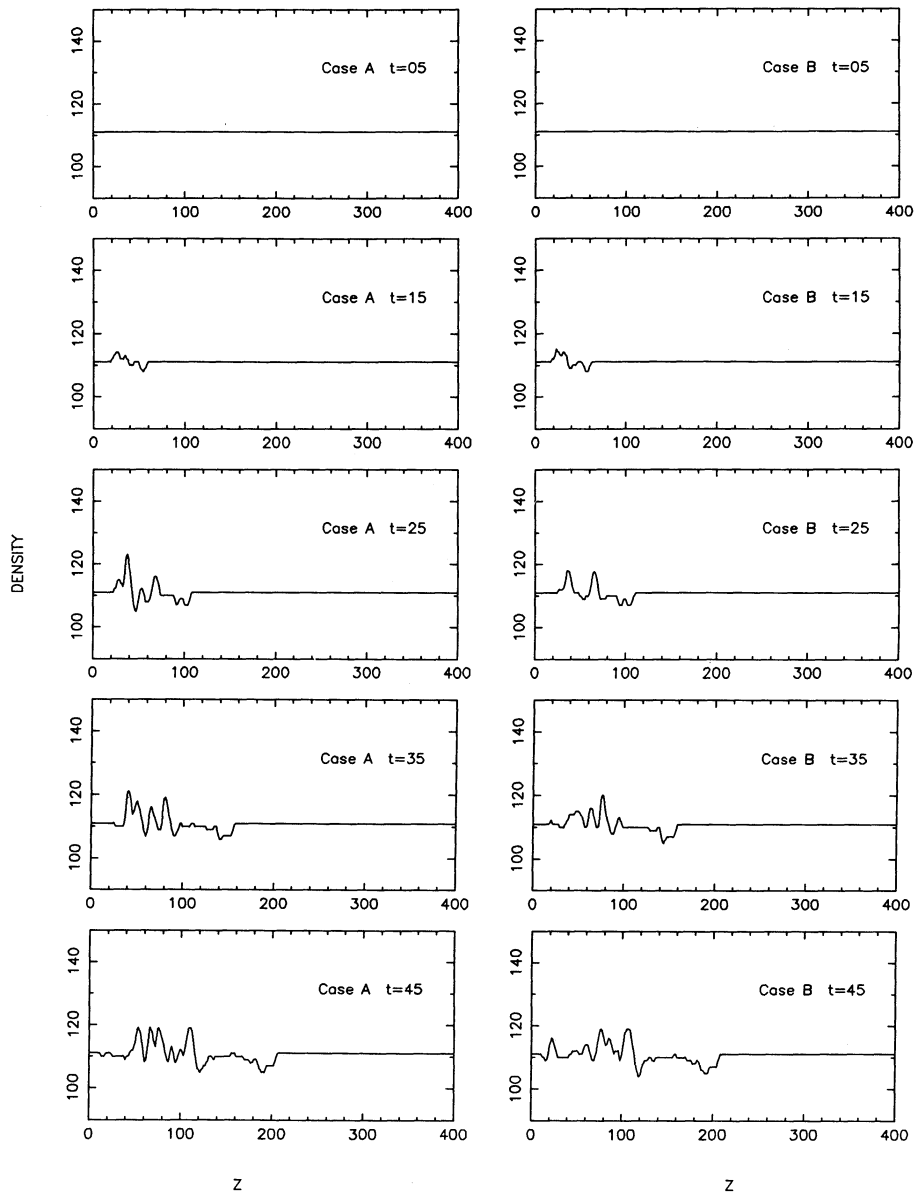

FIG. 4a

FIG. 4.—(*a–b*) Density plots along the jet central axis, made at the times 5, 15, 25, 35, 45, 55, 65, 75, 85, 95 (in units of 4×10^{12} s $\approx 1.27 \times 10^5$ yr), corresponding to cases A and B in Fig. 3.

leads to wiggles in the jet. Then, we begin to see a decollimation of the jet. After $t = 85$, the waves evolve to the nonlinear phase; the wave front becomes stagnant, at which point the jet appears to disrupt (see Fig. 5).

The disruption length ($l_{\rm dspt}$) is $\sim 29R$, where R is the radius of the jet (half width of the slab jet) in both cases A and B, which agrees with NH's measurements. However, the disruption is clearly caused by the intrinsic growing modes associated with the sound wave propagating against the flow and its relevant surface wave modes. The role played in the initial disruption by the imposed sinusoidal oscillation is no more than to excite the intrinsic wave modes. In other words, the jet can be disrupted by internal and surface waves excited by an arbitrary perturbation.

The propagation of the disturbance found in our linear analysis and nonlinear simulations can be understood using the characteristic theory of fluid dynamics which suggests that a small disturbance will propagate along certain characteristic curves in the system. In order to further investigate the disruption process and to estimate the expected disruption length ($l_{\rm dspt}$), we introduce the characteristic theory of fluid dynamics in the following. A jet in a slab geometry can be treated as an isentropic one-dimensional steady flow. Then, one can derive two families of characteristic curves for the system, given by (e.g., Courant & Friedrichs 1948)

$$C^+ : \frac{dz}{dt} = u + a \; ; \tag{1}$$

$$C^- : \frac{dz}{dt} = u - a \; ; \tag{2}$$

where $a = \partial_p / \partial \rho$ is the internal sound speed. The character-

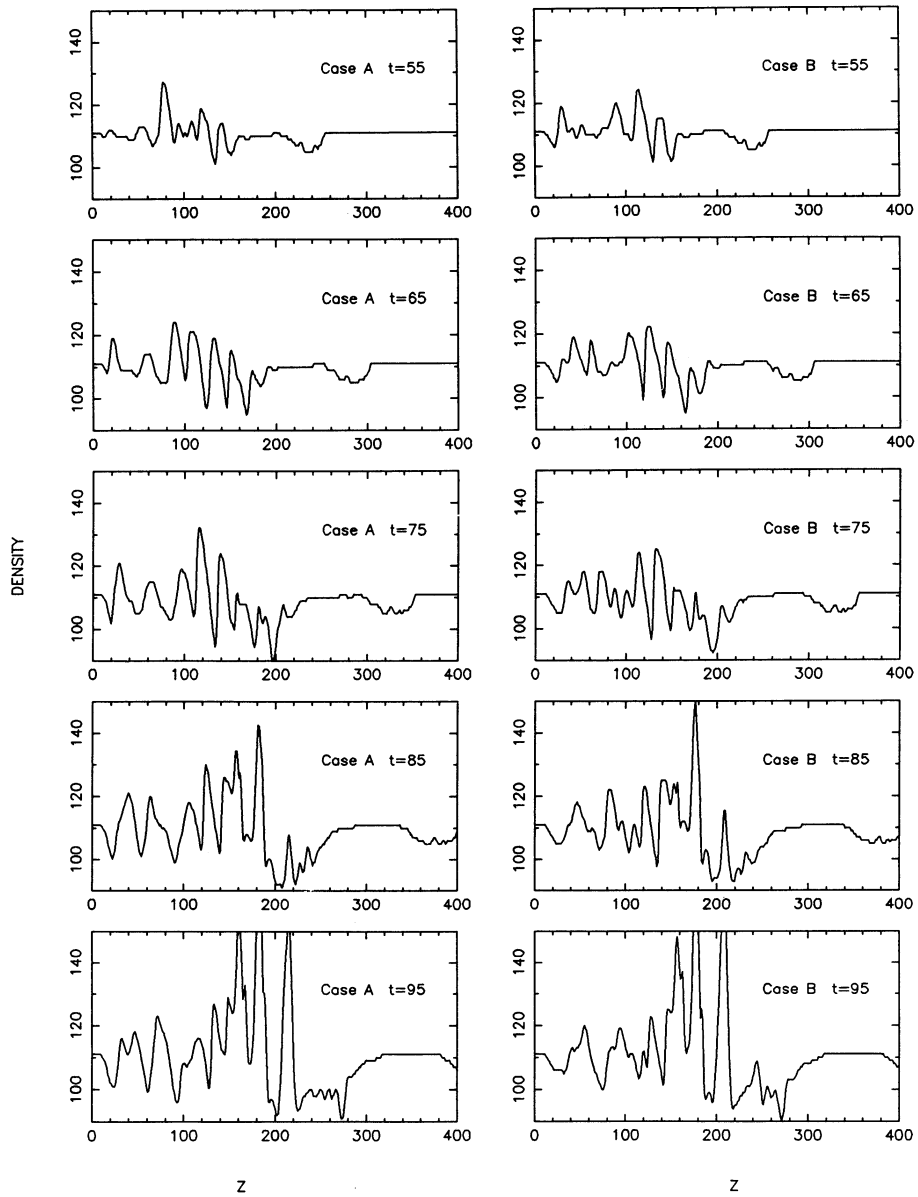

FIG. 4*b*

istics C^+ and C^- in the (t, z)-plane represent motions of a possible disturbance, which correspond to two-body waves found in linear perturbation theory. In a steady flow with a constant velocity (u_0) and an unchanging equation of state $(p_0, \rho_0$, and, therefore, $a_0)$, the characteristic curves in the (t, z)-plane are straight lines with slopes $[(u_0 + a_0)$ and $(u_0 - a_0)]$ assuming that the disturbance does not grow. A perturbation initially imposed at the jet inlet $(t = 0, z = 0)$ will propagate along the lines (C^+ and C^-) in the (t, z)-plane (see Fig. 6). In a thermally confined jet, linear perturbation theory predicts that the normal modes associated with the sound waves will grow. The characteristic lines will be distorted as the waves grow. Assuming the flow is adiabatic, the sound speed $a^2 \propto p/\rho = \rho^{\Gamma-1}$. Thus, "$a$" will increase or decrease as the waves grow (compress or rarefy). The speeds of propagation decrease or increase depending upon the propagation direction of the sound waves and the wave properties.

Assuming that the changes in the propagation velocities are mainly caused by changes in the internal state of the flow, we are able to estimate the propagation velocities corresponding to the C^+ and C^- as follows,

$$C^+ : \frac{dz}{dt} = u_0 + a_0 + a' \; ; \tag{3}$$

$$C^- : \frac{dz}{dt} = u_0 - a_0 - a' \; ; \tag{4}$$

where a' is caused by a small perturbation in density or velocity. We can express $a' = (\Gamma - 1)a_0 \rho'/\rho_0$, and $\rho' = \rho'_0 \exp i(k_R z - w_R t) \exp(-k_I z + w_I t)$ which corresponds to a normal mode of the disturbance. To simplify the following calculations, we trace a fixed phase (say $k_R z - w_R t = 0$) and investigate the maximum spatial growth rate with a fixed real

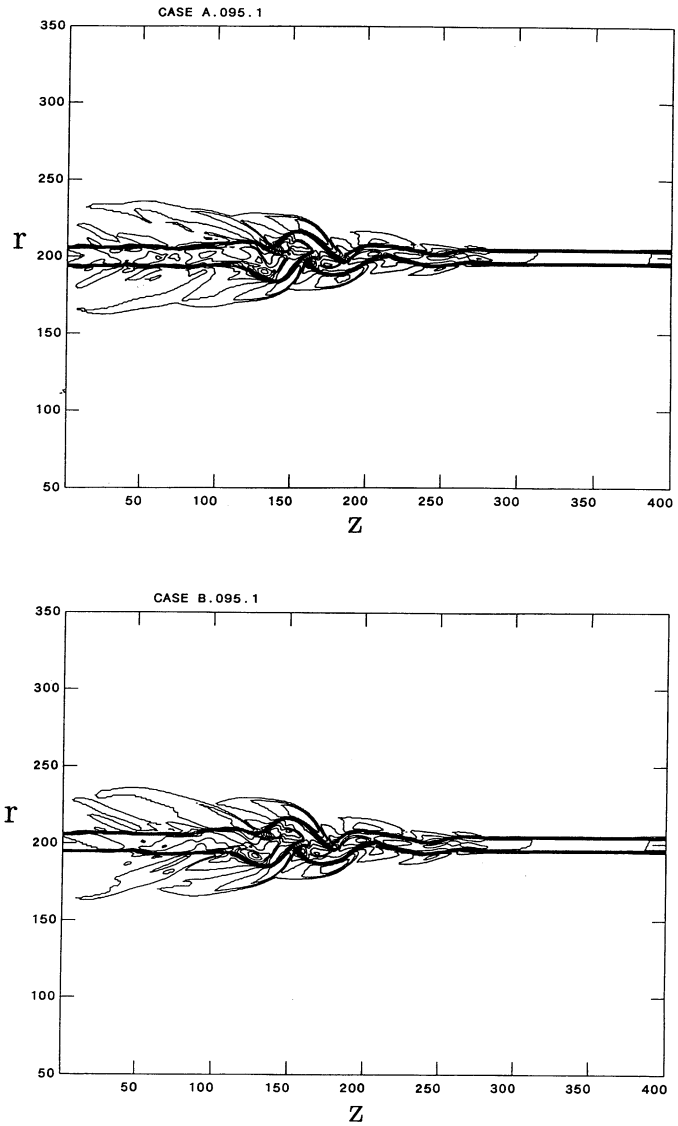

FIG. 5*a*

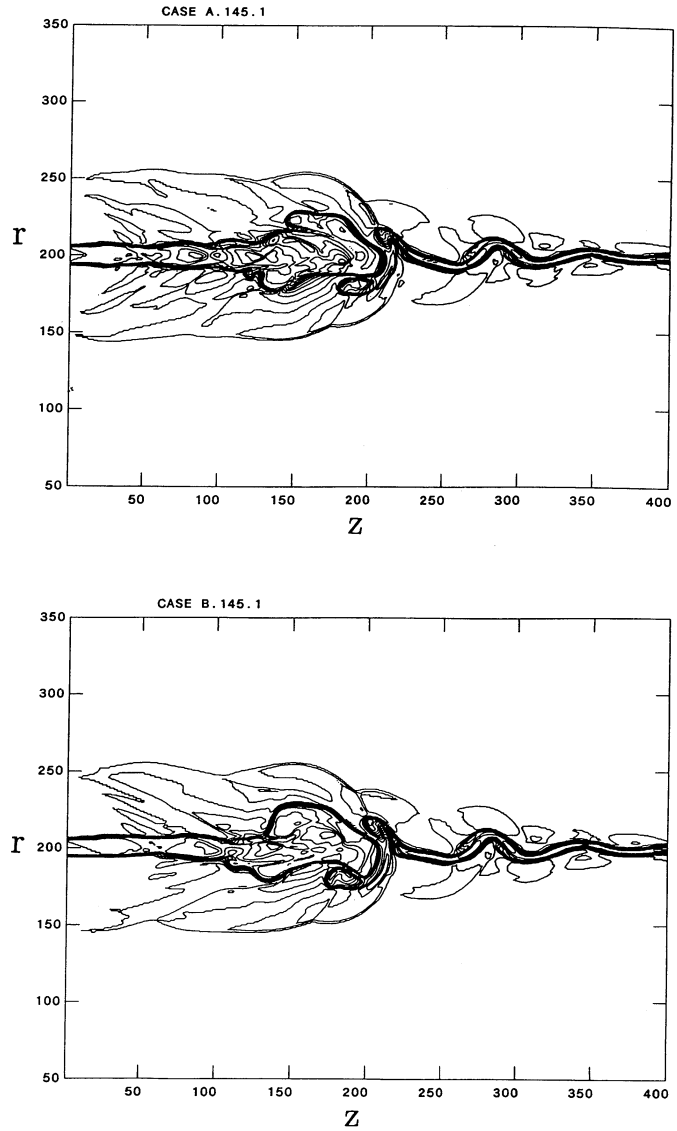

FIG. 5*b*

FIG. 5.—The density contour plots of the numerical simulations with different perturbations (cases A [*top*] and B [*bottom*]) at times (*a*) 95, (*b*) 145, (*c*) 190, (*d*) 235, (*e*) 285 (in units of 4×10^{12} s $\approx 1.27 \times 10^5$ yr).

frequency ($\omega_I = 0$). Thus equations (3) and (4) become

$$C^+ : \frac{dz}{dt} = u_0 + a_0 + (\Gamma - 1)\frac{a_0 \rho_0'}{\rho_0} \exp(-k_I z) ; \quad (5)$$

$$C^- : \frac{dz}{dt} = u_0 - a_0 - (\Gamma - 1)\frac{a_0 \rho_0'}{\rho_0} \exp(-k_I z) ; \quad (6)$$

Because the wave propagating along the C^+ characteristic curve grows slowly and propagates fast in comparison with the one moving along C^-, the decollimation by this wave is less important than the one propagating along C^-. This agrees with our numerical simulations discussed above. Hereafter, we focus on the C^- wave. From equation (6), we expect that the C^- wave slows down quickly as the wave grows.

The stagnation point of this wave (z_s) can be estimated by assuming that the propagation velocity of the wave (not fluid velocity) becomes zero at this point. From our numerical simulations, we find that at the stagnation point, the waves grow significantly and the jet rapidly decollimates. This point appears to mark the transition of the flow from a collimated supersonic jet to a subsonic lobe. Then, from equation (6), we have

$$z_s \approx l_e \ln\left[\frac{(M_{\rm in} - 1)}{(\Gamma - 1)}\frac{\rho_0}{\rho_0'}\right], \quad (7)$$

where $l_e = -k_I^{-1} R$ is the *e*-folding length of a normal mode; ρ_0'/ρ_0 describes the initial perturbation intensity, which can be shown to be $\approx u_r/u_0$ by the continuity equation. For our numerical simulations in Figures 3 and 4 in which $M_{\rm in} = 3$, $\Gamma = 5/3$, and $\rho_0'/\rho_0 \sim u_r/u_0 = 1\%$, we predict $z_s \cong 5.7 l_e$ from equation (7) which is slightly less than the measured disruption length ($l_{\rm dspt} \cong 7 l_e$). Therefore, we are able to present an empirical form for the disruption length ($l_{\rm dspt}$) of a supersonic jet

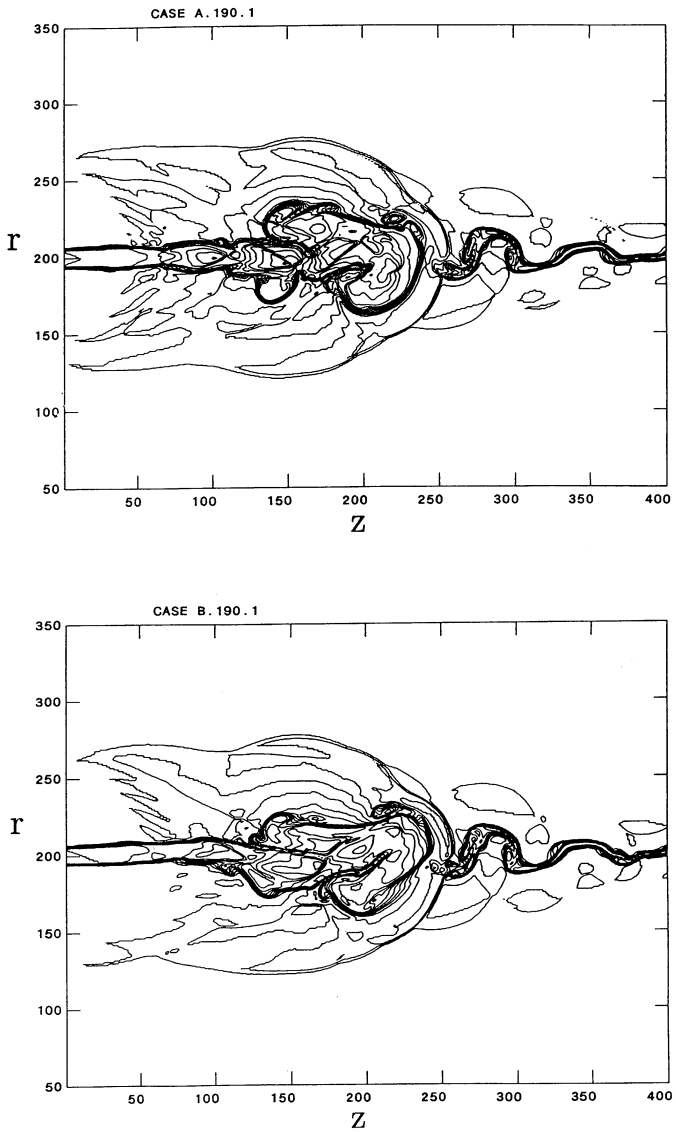

FIG. 5c

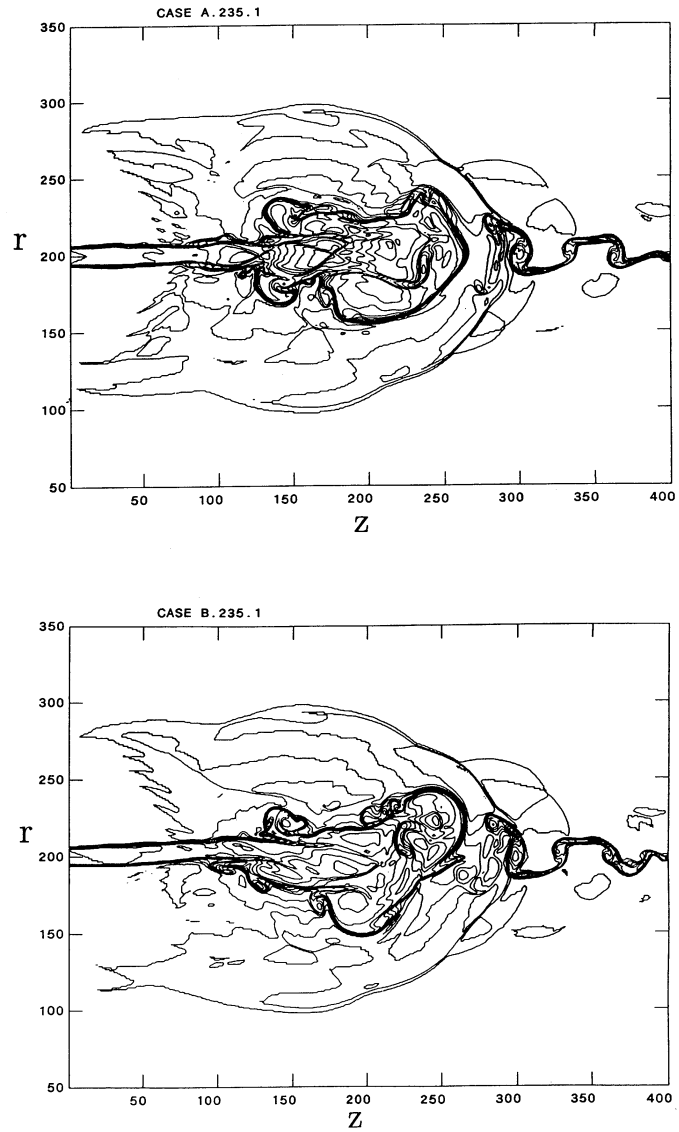

FIG. 5d

caused by a small distrubance

$$l_{\rm dspt} \approx 1.23 z_s = 1.23 l_e \ln\left[\frac{(M_{\rm in}-1)}{(\gamma-1)}\frac{\rho_0}{\rho_0'}\right]. \quad (8)$$

The e-folding length is given by Hardee & Norman (1988) for a resonant mode:

$$l_e^* \approx 1.65\alpha(\eta, M_{\rm in}) R M_{\rm in}\,, \quad (9)$$

where R is the jet radius, and α is a weak function of η and $M_{\rm in}$. (For a highly supersonic jet, $\alpha = 1$; for a slab jet with $M_{\rm in} = 3$ and $\eta = 0.1$, $\alpha = 1.2$). Equation (9) can now be rewritten as

$$l_{\rm dspt} \approx 2RM_{\rm in}\alpha^{-1}\ln\left[\frac{(M-1)}{(\gamma-1)}\frac{\rho_0}{\rho_0'}\right]. \quad (10)$$

The disruption length depends mainly upon the jet Mach number and is only a logarithmic function of the initial perturbation intensity. In VLA observations, the disruption length is measurable. So, from this relation, the jet Mach number can be determined once we estimate the perturbation intensity. In Figure 7, we plot the jet Mach number as a function of disruption length for various perturbation intensities (namely, $\rho_0'/\rho_0 = 20\%, 10\%, 5\%, 2\%, 1\%, 0.5\%, 0.2\%$, and 0.1%).

In this work, we have concentrated on the linear perturbation regime because in most of tailed radio sources, the estimated perturbations (e.g., a parent galaxy moving through intergalactic medium) are $\sim 20\%$ or less (see § 5). Certainly, there are some exceptions in which perturbations to jet flows could be 100% or more. For example, the interaction between two jets observed in 3C 75 (Owen et al. 1985) suggests that other nonlinear interaction processes could be dominant in the jet disruption (Achterberg 1988).

In § 5, we estimate internal Mach numbers for astrophysical jets in tailed sources via the above technique.

3.3. *Jet Structure and Lobe Development at Long Times*

In Figure 5, we present density contour plots at times, $t = 95, 145, 190, 235$, and 285. The initial disruption patterns at $t = 95$ are identical in cases A and B. After long times, the internal reflection wave patterns dominate in the remaining

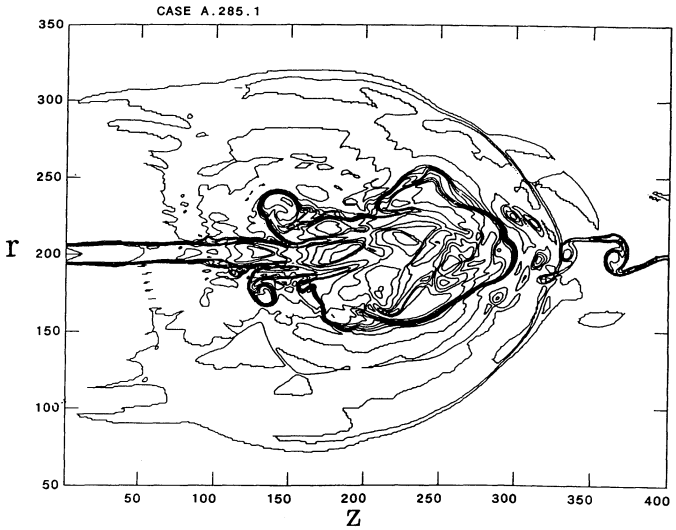

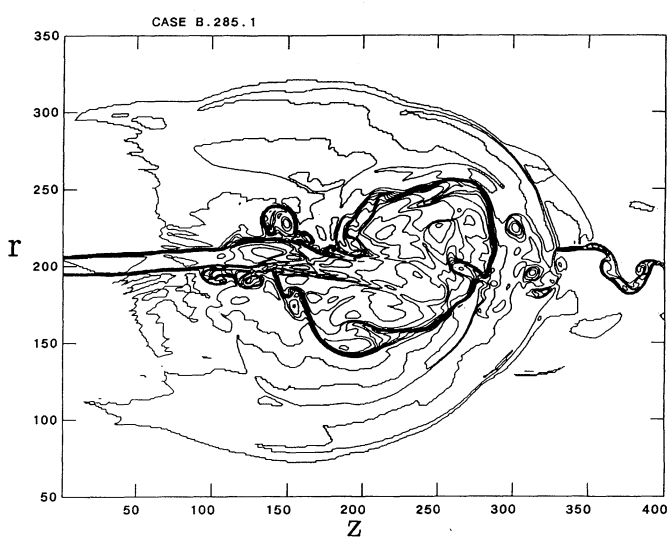

FIG. 5*e*

collimated part of the jet from the jet inlet to $\sim 30\ R$, in both cases A and B. However, the details of the reflection structures in case A are different from case B. In case A, the internal sound waves are reflected off the jet boundaries symmetrically and the reflection waves form weak oblique shocks. These internal oblique shocks interfere around the central axis to produce criss-crossed shock intersections with high gas pressure and high density in case A. Such internal structures have been noted in earlier numerical studies (e.g., Norman et al. 1984). At a long time after initial jet disruption, the jet in case A appears to develop a symmetric pinch surface wave pattern (see $t = 145$, 195, 235, and 285 in Fig. 5) which also was observed by NH (1989) in their run C with a similar driving frequency. In case B, the remaining jet has less symmetric internal structures and internal oblique shocks. From measurements of the z-direction velocity of the flow along the initial jet axis, we find that the z-direction velocity has a transition from supersonic to subsonic around the stagnation point in both cases. After a long time, a lobe or a tail is formed and the shape of the lobes are similar in both cases. Based on our simulations,

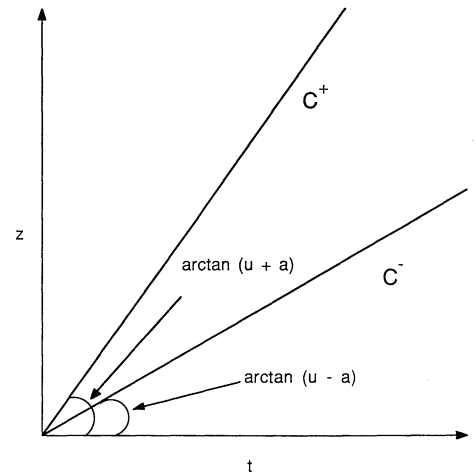

FIG. 6.—Two families of characteristic curve of a one-dimensional, isentropic steady flow.

we conclude that the detailed structures inside the jets depends on the imposed perturbations. Symmetric and/or high-frequency driving perturbations result in symmetric jet structures.

5. ASTROPHYSICAL IMPLICATIONS

In this work, we have shown that the disruption of a supersonic jet can be caused by growing internal body and surface waves propagating against the jet. These waves can be excited by imposing an arbitrary disturbance. As the internal body waves grow, surface waves, predicted by linear theory, are observed in the simulations. It is clear that a perturbation with a regular sinusoidal oscillation seems to be unnecessary to excite the internal body and surface waves.

Many observed astrophysical jets, especially in Fanaroff-Riley (1974) class I (F-R I) sources, are disrupted or decollimated at certain distances from the radio cores. Disturbances such as galaxy merging, shock fronts in supernova explosions, shock fronts at the ISM/ICM interface, the parent galaxy moving through the intracluster medium and so on are all

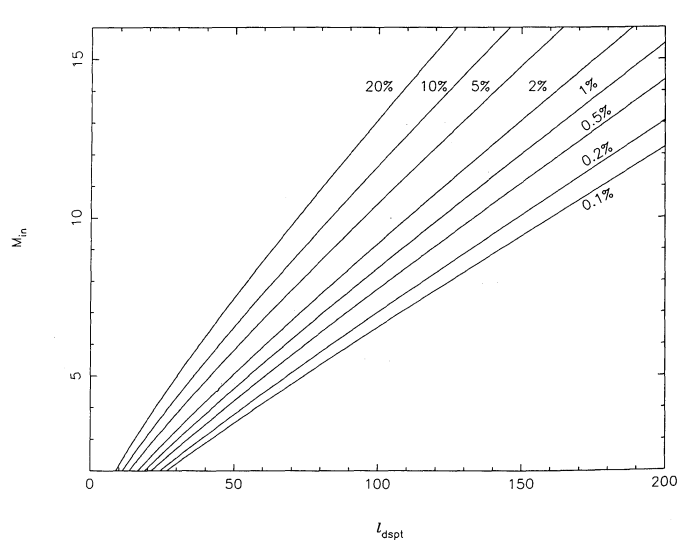

FIG. 7.—Jet Mach number plotted as a function of disruption length (l_{dspt}) for various perturbation intensities (ρ'_0/ρ_0).

possible perturbers that may excite internal body and surface waves in the jet.

In addition, we have distinguished internal sound waves propagating with and against the flow in the numerical simulations. These measured velocities of both sound waves agree quite well with the velocities predicted from linear theory. Similarly the growth of the two waves predicted by linear theory are shown to agree very well with our numerical simulations. We conclude, therefore, that the linear theory is, in general, consistent with numerical simulations. However, it is difficult to identify individual modes predicted by linear theory with the internal body and surface waves in numerical simulations. Actually, these waves are a superposition of all possible modes predicted in the linear theory, which makes it difficult to measure individual modes in numerical simulations. In fact, we do see the reflection pattern in both internal resonant waves, which is related to the reflection modes predicted in the linear theory.

Powerful classical doubles (F-R II sources, e.g., Cygnus A; Dreher, Carrilli, & Perley 1987), are characterized by hot spots at the end of the radio lobe. The jets in classical doubles which terminate at the hot spots are generally interpreted as the "working surface" advancing in the intergalactic medium (e.g., Blandford & Rees 1974; BBR). In the weaker F-R I tailed sources, there is no well-defined boundary at end of the tail. BBR noted that most of the jet bulk kinetic energy in these tailed sources may be dissipated through the channel walls rather than behind a strong shock at the head of the source. The jet may then terminate when the flow becomes transonic. The region of greatest radio emissivity would then be located in the interior rather at the outer extremity of the lobe. Such jet termination has also been observed in propagating jet simulations (Hardee & Norman 1990). The disruption lengths measured in our simulations approximately agree with those in propagating jet simulations (Hardee & Norman 1990). Our analysis of a slab jet complements BBR's argument, helps in understanding the wave instabilities observed in propagating jet simulations, and provides a detailed picture to show how the jet kinetic energy is dissipated through K-H instabilities (where the jet is terminated as body and surface waves grow). The growing internal body waves and the coupled surface waves can explain the quasi-periodic wiggles of jets and the eventual jet disruption. The limb brightened features observed in astrophysical jets may also be related to surface waves which form vortices shedding along the jet surface.

Moreover, this analysis provides a new way to estimate the jet internal Mach number. Equation (10) contains the relation between the disruption length $l_{\rm dspt}$, which is measurable in astronomical observations, and the jet Mach number; $l_{\rm dspt}$ also depends weakly on the perturbation intensity. Let us now pursue examples of how equation (10) can be used on disrupted jet sources in galaxy clusters. The bending of both narrow-angle tailed sources (NAT) and wide-angle tailed sources (WAT) indicates that the outflowing radio plasma substantially interacts with the environment. The bending in NATs can be explained by simple ram pressure arguments (Begelman, Rees, & Blandford 1979, hereafter BRB; O'Dea 1984). In the NATs, the transverse velocity perturbation caused by the motion of the parent galaxy through the intracluster medium could be the dominating factor in exciting internal growing modes in their jets. As can be seen from the previous section, the intensity of the initial perturbation is proportional to the ratio of the parent galaxy velocity to the jet velocity (u_g/u_0). This velocity ratio can be determined via a ram pressure analysis (BRB; 1979). The ratio of the galaxy velocity to the beam velocity in NGC 1265 is $\sim 20\%$, which suggests that the transverse velocity is significant in the excitation of internal wave modes. We also define the disruption length as the distance from the parent galaxy to the point where the jet width increases abruptly. Using the data given by O'Dea & Owen (1986), we find the $l_{\rm dspt}/R$ is 30 and 37 for the east and west jets, respectively, in NGC 1265. Thus, from Figure 7 and assuming $\rho'/\rho \approx u_g/u_0 = 0.2$, we find that the Mach numbers are 5.2 and 6.1 for for the east and west jets, respectively. These results agree quite well with the Mach number determined from ram pressure bending arguments (BRB 1979; O'Dea & Owen 1986).

The problem of bending and disrupting jets in WATs remains unsolved over a decade after WATs were first defined by Owen & Rudnick (1976). WATs are identified with slower moving dominant galaxies at the centers of clusters. Both the jets and tails are generally more luminous than in NATs. It would appear that ram pressure seems insufficient to bend the jets in WATs (Eilek et al. 1984). In addition, new high-resolution VLA observations suggest that none of the jets are significantly bent before disruption in the sample discussed by OOE. Given these characteristics, it would appear that the initial perturbation intensity caused by the motion of the parent galaxies in WATs is much less than that in NATs. However, the wiggles and flares which precede the abrupt jet disruption (e.g., 0110+152 in OOE) strongly indicate that the jets must be subject to an instability caused by a growing internal body wave and its coupled surface wave that may be excited by a very small perturbation. The velocity of a cD galaxy, often associated with WATs, with respect to the cluster centroid is probably 100 km s^{-1} (Burns 1986). Thus, velocity perturbations from the parent galaxies are $\sim 1\%$. Therefore, other kinds of perturbation, such as irregularity of feeding gas into jets from radio cores, or shocks at the ISM/ICM interface (e.g., Norman, Burns, & Sulkanen 1988) may become important.

Another method for estimating the perturbation intensity involves the density distribution along the jet plotted from our simulations (Fig. 5). We find that the ratio of the standard deviation to the average of the density ($\sigma_\rho/\bar{\rho}$) along the jet axis is about a factor of 10 higher than the initial perturbation (ρ'/ρ_0). Furthermore, for VLA jets, the equipartition minimum pressure along the jet determined from the surface brightness of the radio maps can be used to estimate ρ'/ρ_0 as follows:

$$\rho'/\rho_0 \approx f^{-1}(\sigma_\rho/\bar{\rho}) \approx f^{-1}\Gamma^{-1}(\sigma_p/\bar{p}) , \qquad (11)$$

where $\bar{p}$ is the averaged jet pressure; σ_p is the standard deviation of the pressure; $\Gamma = 5/3$, the adiabatic index; and f is the growth factor of the jet density. Assuming that the growth factor is $f = 10$ in wide-angle tailed sources, then, we are able to determine the jet internal Mach numbers in WATs by measuring the disruption length and the ratio of the standard deviation to the average of the minimum pressure along the jet axis. OOE have provided some measurements for the determination of disruption lengths and the ratio $\sigma_p/\bar{p}$ of these jets in their WAT sample. Unfortunately, in most cases, the resolutions in their observations were not sufficient to determine the jet widths, so the pressure and the value of $l_{\rm dspt}/R$ for the jets in OOE's sample are uncertain. In 0110+152, the upper limit of $l_{\rm dspt}/R$ is 64 and 55 for the north and south jets, respectively. If we estimate the initial perturbation intensity

$\rho'/\rho_0 \approx 0.02$, then the lower limits of the Mach numbers are 6.5 and 5.7 for the north and south jets, respectively.

In 3C 449 (Perley et al. 1979; Cornwell & Perley 1984), the radio source is associated with the cD galaxy in the open cluster Zw 2231.2+3732. The jets on both sides of the nucleus are remarkably straight. Each jet wiggles and abruptly disrupts at $\sim 80''$ from the nucleus. The $l_{\rm dspt}/R$ is ~ 34 and 41 for the north and south jets, respectively, where the average jet width, $2R$, is 4".7 and 3".9. Using equation (11) and measurements given by Cornwell & Perley (1984), we estimate $\rho'/\rho_0 \approx 0.023$ and 0.027 for the north and south jets, respectively. Thus, we find that the average jet Mach numbers are ~ 3.8 and 4.5 for the north and south jets, respectively, in 3C 449.

We are aware that cylindrical geometry is closer to practical astrophysical jets than slab geometry, and there are some differences between cylindrical and slab jets. In Paper I, we suggested that the first symmetric and antisymmetric reflection modes are dominant in the growing waves in a jet. Linear analysis of instabilities indicated that in general, the spatial modes of a cylindrical jet grow faster than those in a slab jet but there are no significant differences in *e*-folding length between a slab instability and a cylindrical instability for the reflection modes (Hardee & Norman 1988). We note that the errors in determining jet Mach numbers caused by the slab geometry are no more than 10%.

Also, the uncertainty of the projection angle between a jet and the sky results in an underestimate of the disruption lengths. Consequently, the jet Mach numbers are underestimated in the previous discussion.

We note that a practical astrophysical jet is more complicated than the model discussed in this paper. For instance, an expanding, supersonic jet may be subject to acceleration of the flow. Also, turbulent entrainment seems very likely in astrophysical jets (Bicknell 1984; De Young 1986), which may decelerate the jets. Nevertheless, the disruption of astrophysical jets is an important signature of the wave instabilities in the jets. The detailed fluid processes, such as expansion and entrainment, need to be quantitatively investigated in further theoretical and numerical studies.

With the above caveats in minds, we conclude the following concerning WATs: (1) the jets observed in WATs must be at least mildly supersonic; (2) the abrupt jet disruption may be caused by growing internal body waves propagating against the flow and their coupled surface waves; (3) the observed wiggles and flares in the jet prior to the disruption signals the presence of the growing waves; (4) the jet flows are subject to subsonic transition during the disruption; and (5) the tailed flows in WATs are subsonic and are, thus, easier to bend.

6. SUMMARY AND CONCLUSIONS

In Paper I, we solved the dispersion relation for a thermally confined slab jet in the complex (k, ω) domain. Our analysis demonstrated an association of the physical waves with unstable modes in the system. This work is also a useful complement to previous studies of the comprehension of the wave phenomena in jets. An understanding of the wave characteristics is crucial for comparing linear theory with simulations and observations. We note that the linear study of a thermally confined slab jet provides the fundamental physics to understand the features appearing in the numerical simulations and astronomical observations, although it is not a perfect model to fit a specific observed jet.

Instabilities and disruptions of jets have now been seen in both radio observations and numerical simulations. In the present work, we have established a number of important points regarding the instability of body and surface waves in a jet. The growing body waves should be dominant in the linear stage of evolution of jet instabilities. The two waves are distinguishable by their average velocity, $u_0 - a_{\rm in}$ and $u_0 + a_{\rm in}$. In fact, the body and the relevant surface waves propagating against the flow had been observed as a fast-growing wave pattern in previous jet simulations (Norman et al. 1984). In our new numerical simulation, we demonstrated that the internal body and surface waves can be excited by a general but simple perturbation rather than a regular sinusoidal oscillation. The fast propagating wave pattern is a rarefied wave with an average velocity $\sim 1.33\ u_0$ in a Mach number 3 jet, which agrees very well with linear theory. The observed slow propagating wave pattern grows fast. The coupled body and surface waves appear as wiggles, and propagation slows as they grow. These waves eventually disrupt the jets. Using a characteristic curve analysis, we showed that the disruption length is simply related to the jet Mach number and the perturbation intensity. Thus, the Mach number for a radio jet can, in principle, be determined by measuring the disruption length and estimating the perturbation intensity. The jet Mach numbers in narrow-angle and wide-angle tailed sources determined in this way agree quite well with ones obtained from ram pressure bending arguments. We conclude that the jets observed in tailed radio sources must be mildly supersonic. The wiggles and flares in the jets prior to the disruption (or jet/tail transition) signal the growth of internal body and surface wave modes.

We thank D. Clarke for his help in setting up the numerical simulations, T. Cornwell for providing us with his 3C 449 radio data, and A. O'Donoghue for providing the contour map of 0110+152. We also thank P. E. Hardee, F. N. Owen, J. Eilek, and R. Perley for their useful comments. J.-H. Z. wishes to acknowledge the University of New Mexico for support during the course of this Ph.D. thesis research. This work was supported by NSF grants AST-8611511 and AST-9012353 to J. O. B. and M. L. N.

REFERENCES

Achterberg, A. 1988, A&A, 191, 167
Arnold, C. N., & Arnett, W. D. 1986, ApJ, 305, L57
Begelman, M. C., Blandford, R. D., & Rees, M. J. 1984, Rev. Mod. Phys. 26, 255 (BBR)
Begelman, M. C., Rees, M. J., & Blandford, R. D. 1979, Nature, 279, 770
Bicknell, G. V. 1984, ApJ, 286, 68
Blandford, R. D., & Rees, M. J. 1974, MNRAS, 169, 395
Burns, J. O. 1986, Canadian J. Phys., 64, 373
Clarke, D. A., Norman, M. L., & Burns, J. O. 1986, ApJ, 311, L63
———. 1989, ApJ, 342, 700
Cornwell, T., & Perley, R. 1984, in Proc. NRAO Workshop 9, Physics of Energy Transport in Extragalactic Radio Sources, ed. A. H. Bridle & J. A. Eilek (Greenbank: NRAO), 39
Courant, R., & Friedrichs, K. O. 1948, in Supersonic Flow And Shock Waves (New York: Interscience)
Cox, C. I., Gull, S. F., & Scheuer, P. A. G. 1991, preprint
De Young, D. S. 1986, ApJ, 307, 62
Dreher, J. W., Carrilli, C. L., & Perley, R. A. 1987, ApJ, 316, 611
Eilek, J. A., Burns, J. O., O'Dea, C. P., & Owen, F. N. 1984, ApJ, 278, 37
Fanaroff, B. L., & Riley, J. M. 1974, MNRAS, 167, 31P

Ferrari, A., Trussoni, E., & Zaninetti, L. 1981, MNRAS, 196, 1054
Gaster, M. 1965, J. Fluid Mech., 22, 433
Hardee, P. E., & Norman, M. L. 1988, ApJ, 334, 70
———. 1990, ApJ, 365, 134
Hardee, P. E., Norman, M. L., Koupelis, T., & Clarke, D. A. 1992, ApJ, submitted
Jones, T. N. & Owen, F. N. 1979, ApJ, 234, 818
Lind, K. R., Payne, D. G., Meier, D. L., & Blandford, R. D. 1989, ApJ, 344, 89
Matthews, A. P., & Scheuer, P. A. G. 1990a, MNRAS, 242, 606
———. 1990b, MNRAS, 242, 640
Miley, G., Perola, G., van den Kruit, P., & van der Laan, H. 1972, Nature, 237, 269
Norman, M. L., Burns, J. O., & Sulkanen, M. 1988, Nature, 335, 146
Norman, M. L., & Hardee, P. E. 1988, ApJ, 334, 80
Norman, M. L., Smarr, L., Winkler, K.-H. A., & Smith, M. D. 1982, A&A, 113, 285
Norman, M. L., & Winkler, K. H. 1986, in Astrophysical Radiation Hydrodynamics, ed. K.-H. Winkler & M. L. Norman (Dordrecht: Reidel), 182
Norman, M. L., Winkler, K. H., & Smarr, L. L. 1984, in Proc. NRAO Workshop 9, Physics of Energy Transport in Extragalactic Radio Sources, ed. A. H. Bridle & J. A. Eilek (Greenbank: NRAO), 150
O'Dea, C. P., & Owen, F. N. 1986, ApJ, 301, 84
O'Donoghue, A. A., Owen, F. N., & Eilek, J. A. 1990, ApJS, 72, 75
Owen, F. N., O'Dea, C. P., Inoue, M., & Eilek, J. A. 1985, ApJ, 294, L85
Owen, F. N., & Rudnick, L. 1976, ApJ, 203, 307
Payne, D. G., & Cohn, H. 1985, ApJ, 291, 655
Perley, R. A., Bridle, A. H., & Willis, A. G. 1984, ApJS, 54, 291
Perley, R. A., Willis, A. G., & Scott, J. S. 1979, Nature, 281, 437
Scheuer, P. A. G. 1974, MNRAS, 166, 513
Smith, M. D., Norman, M. L., Winkler, K.-H. A., & Smarr, L. 1985, MNRAS, 214, 67
Williams, A. G., & Gull, S. F. 1984, Nature, 310, 33
———. 1985, Nature, 313, 34
Wilson, M. J., & Falle, S. A. E. G. 1983, MNRAS, 216, 971
Zhao, J.-H., Burns, J. O., Hardee, P. E., & Norman, M. L. 1992, ApJ, 387, 69, (Paper I)